

# Analysis of Frequency Leakage in Different Optical Paths of Nano-Metrology Systems Based on Frequency-Path Models

S. Olyaei\*, Z. Dashtban

Nano-Photonics and Optoelectronics Research Laboratory (NORLab), Shahid Rajaee Teacher Training University (SRTTU), Lavizan, Tehran, I. R. Iran

(\* ) Corresponding author: s\_olyaei@srttu.edu  
(Received: 22 July 2013 and accepted: 28 Jan. 2014)

## Abstract:

*The drawing of frequency-path (F-P) models of optical beams is an approach for nonlinearity analysis in nano-metrology systems and sensors based on the laser interferometers. In this paper, the frequency-path models of four nano-metrology laser interferometry systems are designed, analyzed and simulated, including conventional and modified two- and three-longitudinal-mode laser interferometers. The frequency-path model can be used for nonlinearity error analysis resulting from imperfect alignment of optical head and non-ideal laser polarization states. The number of active F-P element in these systems is calculated by multiplying the number of frequency and paths. The number of active F-P elements for conventional and modified two-mode laser interferometer is 4, and this is 6 for conventional and modified three-mode laser interferometer. The output interference terms can be calculated from the active F-P elements which is 10 for conventional and modified two-mode interferometer and is 21 for conventional and modified three-mode one. The interference terms include optical power, ac interference, dc interference, and ac reference. These terms are also investigated in zero (fixed target), low (2mm/s), and high (20mm/s) target velocities using frequency spectrum of photocurrents.*  
**Keywords:** Frequency-path model, Interference terms, Heterodyne interferometer, Nano-metrology, Frequency spectrum.

## 1. INTRODUCTION

Measurement of optical displacements based on interferometry was first introduced by Michelson in 1881. Since then, dynamic range and measurement accuracy of displacement have been enhanced by introducing the new heterodyne laser interferometers. The need for more accuracy in measurement has recently increased significantly as a result of some progressions in nano-metrology, such as semiconductor metrology and lithography applications [1, 2]. The two-mode heterodyne laser interferometer was first proposed in the 1970s. This new interferometry is used extensively in several

varieties of applications to measure displacements in the range of less than 1 nm to 60 m [3, 4]. Some of the earlier applications are described by Dahlquist et al. [5], Dukes and Gordon [6], and Eberhardt and Andrews [7].

The laser interferometers for displacement measurement are mainly categorized into homodyne and heterodyne. The homodyne interferometer uses one-frequency laser and it can encode the displacement in the amplitudes of the fringe signals. On the other hand, heterodyne interferometer uses two- or multi-mode laser, hence the displacement is encoded in the phase of the beat signal of the multiple-frequency waves. The heterodyne interferometer

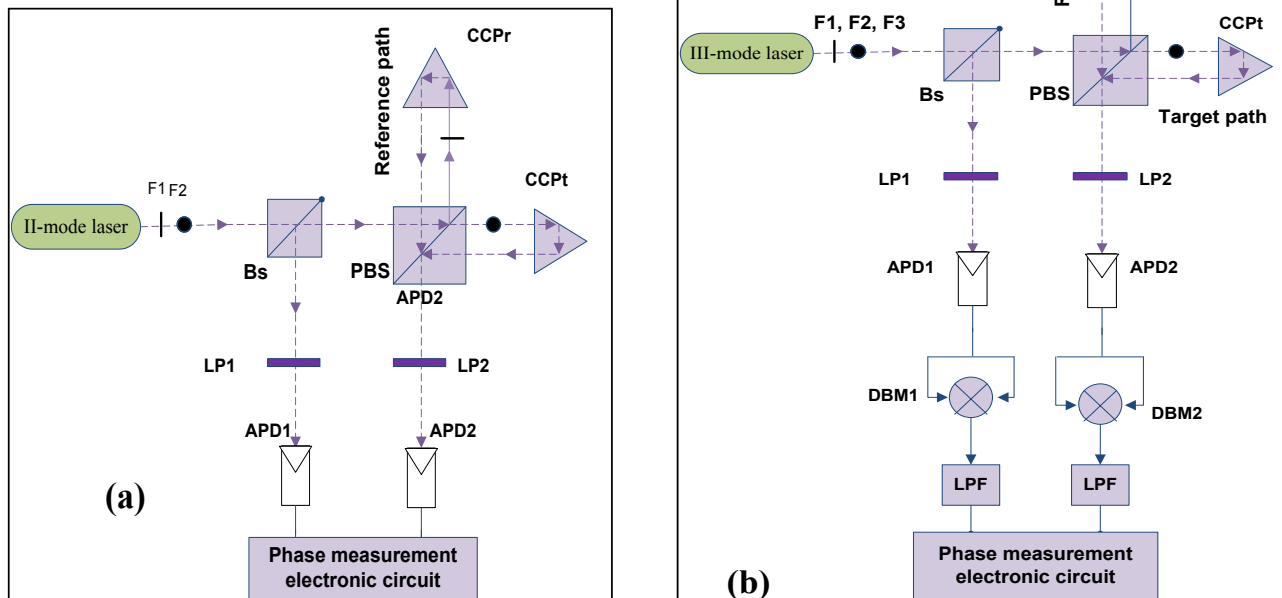


**Figure 1:** The conventional (a) two-longitudinal-mode and (b) three-longitudinal-mode He-Ne laser interferometers. BS: beam splitter, PBS: polarizing beam splitter, CCP: corner cube prism, LP: linear polarizer, APD: avalanche photodiode, DBM: double-balanced mixer, LPF: low-pass filter.

can be widely used for precision length measuring, positioning systems, and other related parameters [8-14], because of a high signal-to-noise ratio and an easy alignment [15]. It is also highly sensitive and has a linear relation between the phase of measuring object and the interferometer output. These features make heterodyne interferometry preferable to other interferometry. Whereas, it has the disadvantage of more complicated phase encoding electronics and more nonlinearity error compared with the homodyne interferometer. In the heterodyne systems, non-ideal distinction between two frequencies through different optical paths produces the first and second order periodic nonlinearity errors. Several primary researches were proposed about the error of heterodyne interferometer [16-24].

The accuracy is mainly limited by the nonlinearity which comes from an imperfection of laser beam, optical components, and phase-measuring electronic system. Quenelle first predicted the nonlinearity

in the heterodyne interferometer [25], and Sutton verified it experimentally [3]. Wu and Deslattes provided the analytical models of nonlinearity effects in the heterodyne interferometer in detail [26]. Several methods have been proposed to reduce the nonlinearity errors [1, 15, 19, 20, 27]. In order to increasing resolution, Gue *et al.* represented a system in which the resolution was increased by twofold without requiring doubled optical path length in the measurement [28].

Meanwhile using super-heterodyne interferometer arrangement causes increase in resolution, the three-mode heterodyne interferometer is being used. This was first reported by Yokoyama *et al.* in 2001 [29] and then was improved in 2005 for unlimited target velocity [30]. On the other hand, using three-mode heterodyne laser interferometer causes the resolution increase with regard to the two-mode heterodyne interferometer [31, 32].

A design of a kind of three-mode heterodyne interferometer with a fourfold resolution rather than

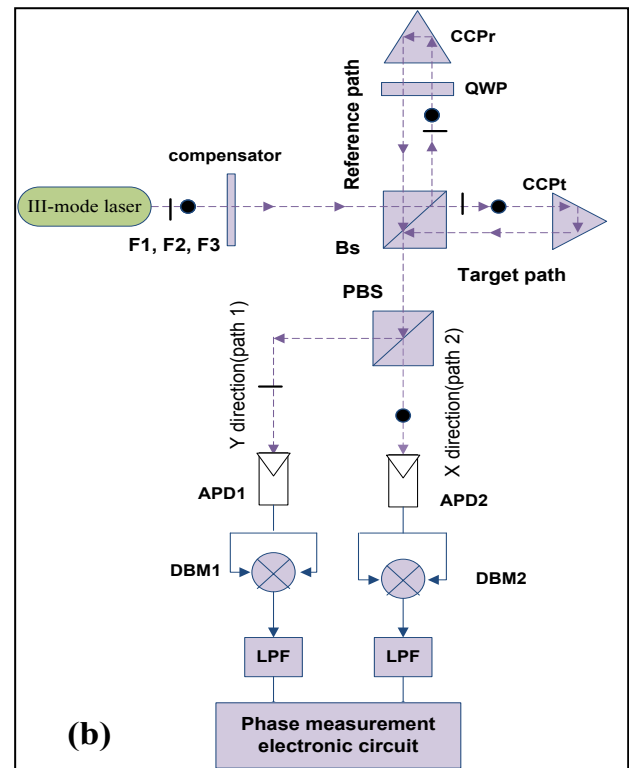
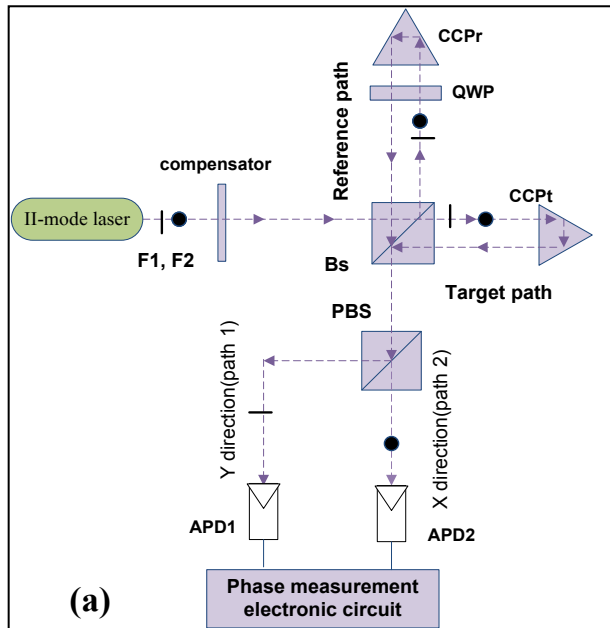


**Figure 2:** The modified (a) two-longitudinal-mode and (b) three-longitudinal-mode He-Ne laser interferometers. BS: beam splitter, PBS: polarizing beam splitter, CCP: corner cube prism, LP: linear polarizer, APD: avalanche photodiode, DBM: double-balanced mixer, LPF: low-pass filter, QWP: quarter-wave plate.

the two mode heterodyne interferometer or double resolution compared to three-mode heterodyne interferometer is a sample of recently extensive advances in the field of nanometrology. Also, a kind of three-mode heterodyne laser interferometer with quadrupled resolution was presented in 2011 [33]. The optical head of the system presented in [33] is similar to the optical heterodyne interferometer reported by Guo *et al.* [28], but a three-mode laser as a light source was used to increase the resolution. The drawing of frequency-path (F-P) models of optical beams is an approach for representing frequency leakage error in different paths [24, 34-37]. In this paper, we designed and analyzed F-P model and nonlinearity error terms for four kinds of interferometer systems including conventional and modified two- and three-mode laser interferometers. We also wrote the equations of the nonlinearity errors resulting from non-ideal polarizing beam splitter for each of the systems implied and compared each of

which in terms of the number of interference term and F-P elements. The interference terms were also described by drawing the frequency spectrum of photocurrents in zero, low (2mm/s), and high (20mm/s) target velocities.

## 2. ANALYSIS OF FREQUENCY LEAKAGE IN DIFFERENT OPTICAL PATHS

### 2.1. Discussion of four nano-metrology laser interferometry systems

In this section four nano-metrology systems based on laser interferometry are introduced. The electrical field equations and frequency-path models will be easier with a brief description of the four systems. In Figure 1, the conventional two- and three-longitudinal-mode He-Ne laser interferometers are shown. The optical head consists of the base

**Table 1:** A comparison between F-P models of four nano-metrology systems.

	Conventional two-mode	Modified two-mode	Conventional three-mode	Modified three-mode
Active F-P element	4	4	6	6
Optical power	4	4	6	6
AC Interference	2	2	6	6
DC Interference	2	2	3	3
AC Reference	2	2	6	6

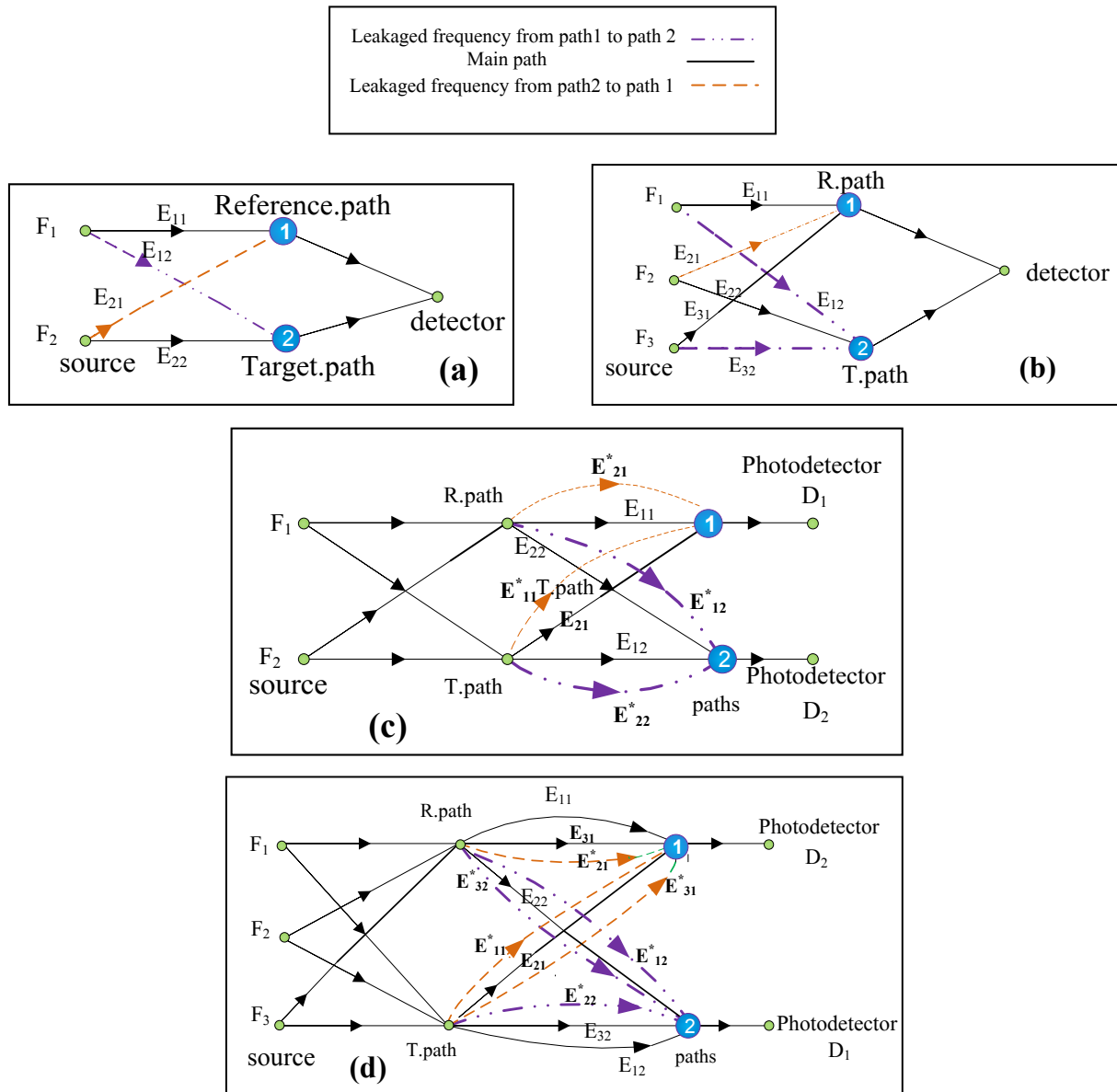


**Figure 3:** The F-P model for (a) conventional two-mode [34], (b) conventional three-mode, (c) modified two-mode, and (d) modified three-mode interferometers.

and measurement arms. The laser output beams are first separated by a beam splitter (BS) and then is directed to the base and measurement arms. In the measurement arm, the beams are split into two subsequent beams by polarizing beam splitter (PBS) and finally are directed to each path of the interferometers.

Figure 2 shows the block diagram of the modified two- and three-mode laser interferometer with

doubled and quadrupled resolution with respect to the conventional two-mode laser interferometer. In this condition, optical head is different from conventional case. The laser output beam is split into two paths with a beam splitter (BS). In the reference path (of the measured arm), a quarter-wave plate with its fast axis  $45^\circ$  off the x-direction and a corner cube prism (CCP) were used to rotate the incident x- (or y-) polarization into its orthogonal y- (or x-) orientation

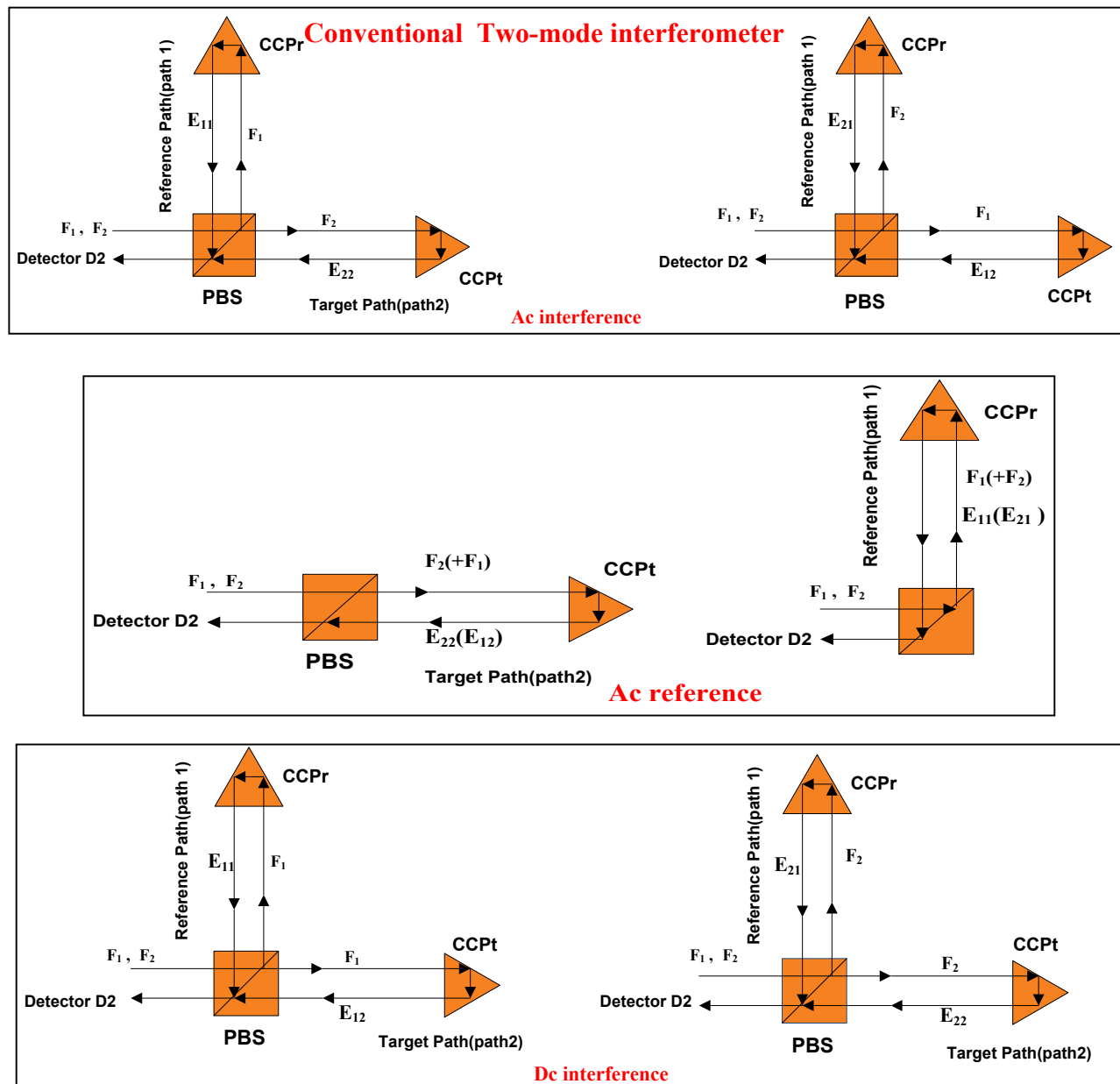


Figure 4: The schematic of interference terms for conventional two-mode interferometer.

[28]. The wave plate output was then recombined with the returned beam from the other path at the BS. Meanwhile, the polarizations of returned beam were separated by PBS [28, 33]. After the PBS, two photodetectors namely  $APD_1$  and  $APD_2$  were used in order to detecting base and measurement signals, respectively.

## 2.2. Frequency–path model

The non-ideal separation of output laser beams incurs the first and second order periodic errors of the heterodyne interferometers [35]. The drawing of F-P models of optical beams is an approach for

representing frequency leakage error in different optical paths [27, 34, 36, 37].

In the F–P modeling, the electric field domain of each F–P element is described by the letter E with two subscripts. The first subscript denotes the source frequency, while the second lists the path from the source to detector. The squaring operation of the photocurrents produces  $q(q+1)/2$  distinct interference terms, where  $q$  is the number of active F–P element that is calculated by multiplying the number of frequencies and paths [34]. The distinct interference terms can be divided into four groups namely dc interference, ac interference, ac reference,

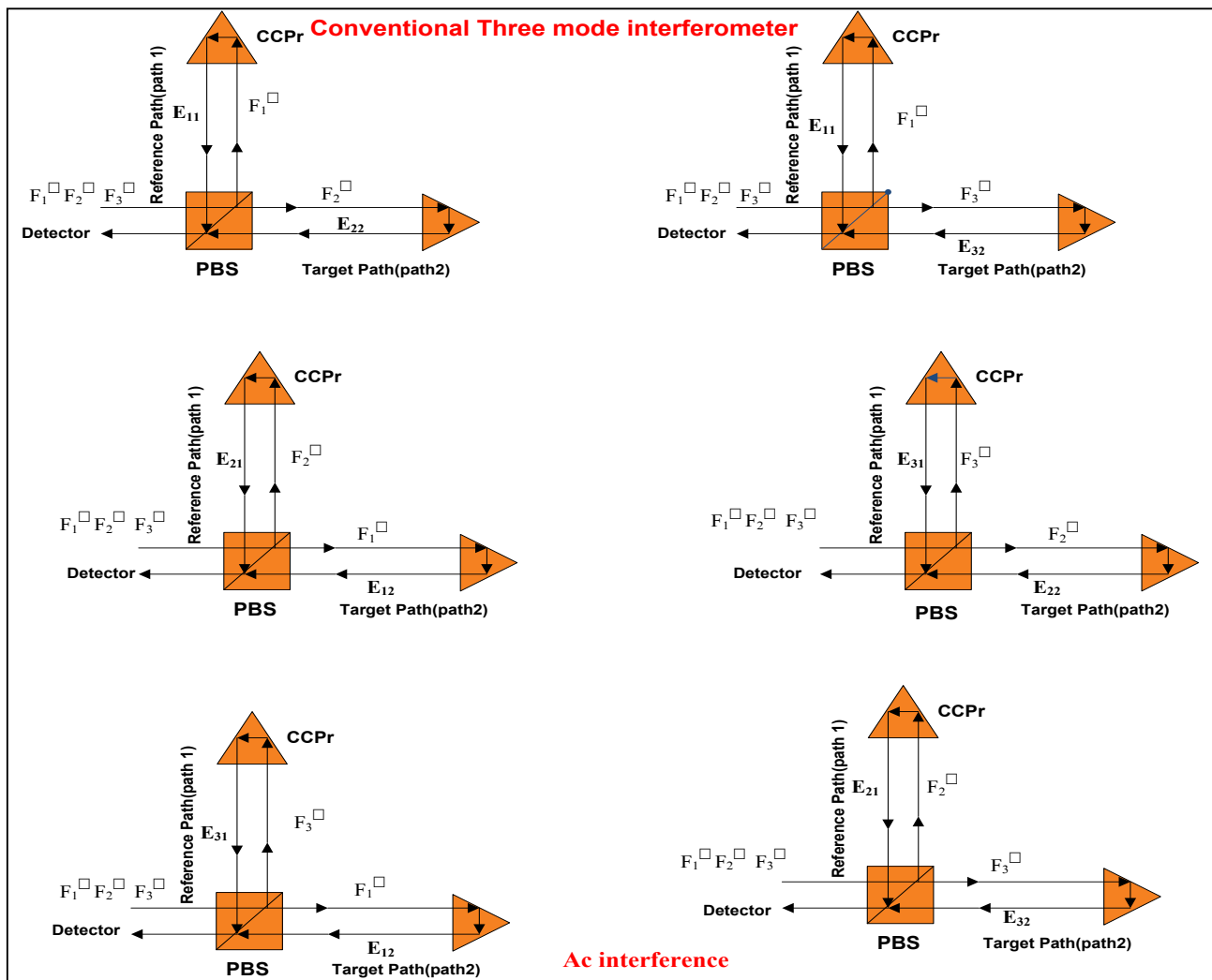


**Figure 5:** The schematic of interference terms for conventional three-mode interferometer (part 1)

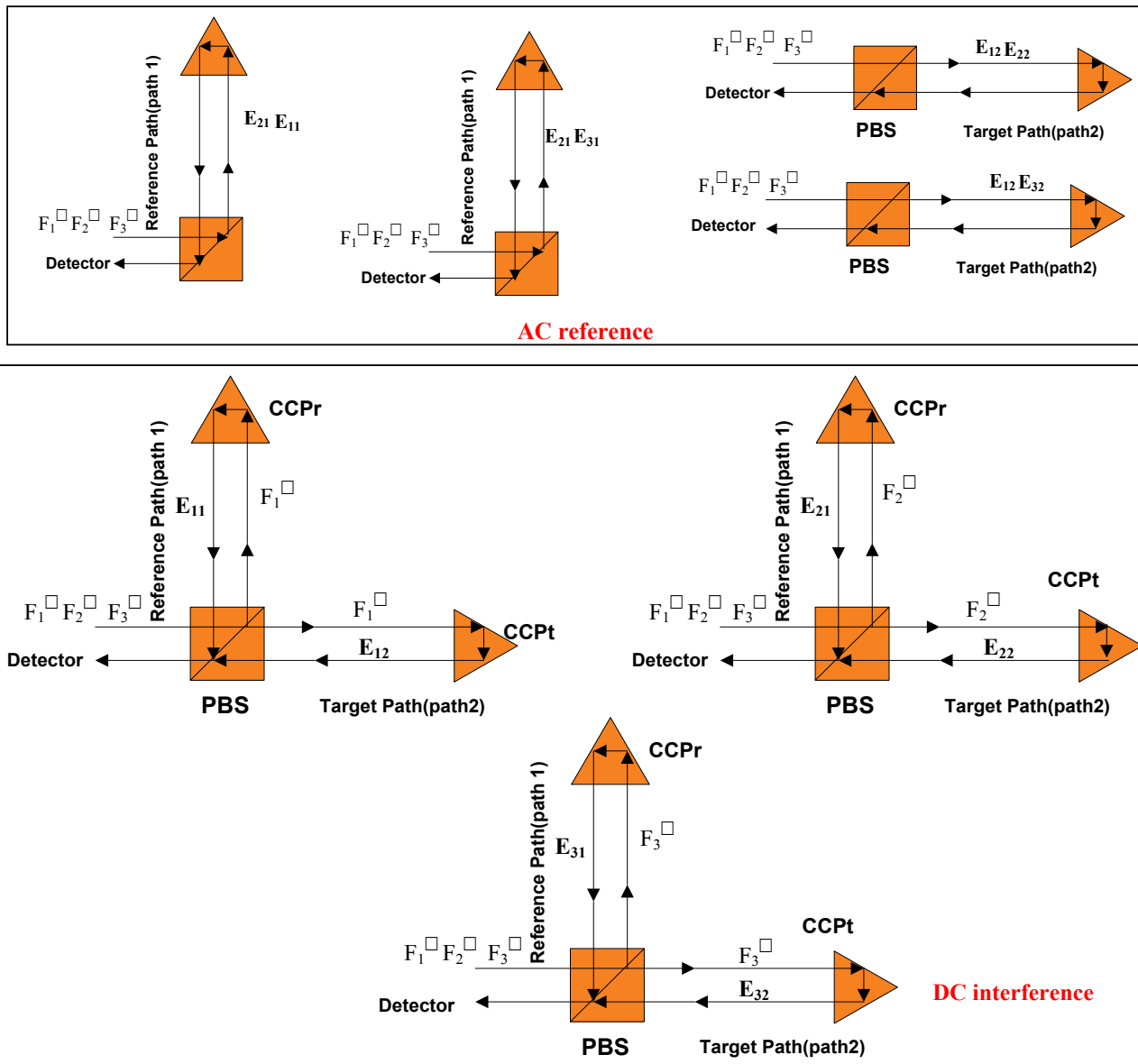


**Figure 5:** The schematic of interference terms for conventional three-mode interferometer (part 2)

and optical power [34-36].

In Figure 3, the F-P models for four interferometer systems including conventional and modified two- and three-mode interferometers are demonstrated. The electrical fields of the two- and three-mode laser output are described as:

$$E = E_i \cos \omega_i t \quad (1)$$

Where  $E_i$  is used to represent the electrical field

amplitude and  $\omega_i$  is the angular optical frequency, ( $i = 1, 2$  for two-mode and  $i = 1, 2, 3$  for three-mode type).

### 2.2.1. F-P model of conventional two-mode interferometer

In the reference path (path 1) of conventional two-mode interferometer,  $f_1$  is the main frequency and  $f_2$  is the leakage, as a result the fields existing in this

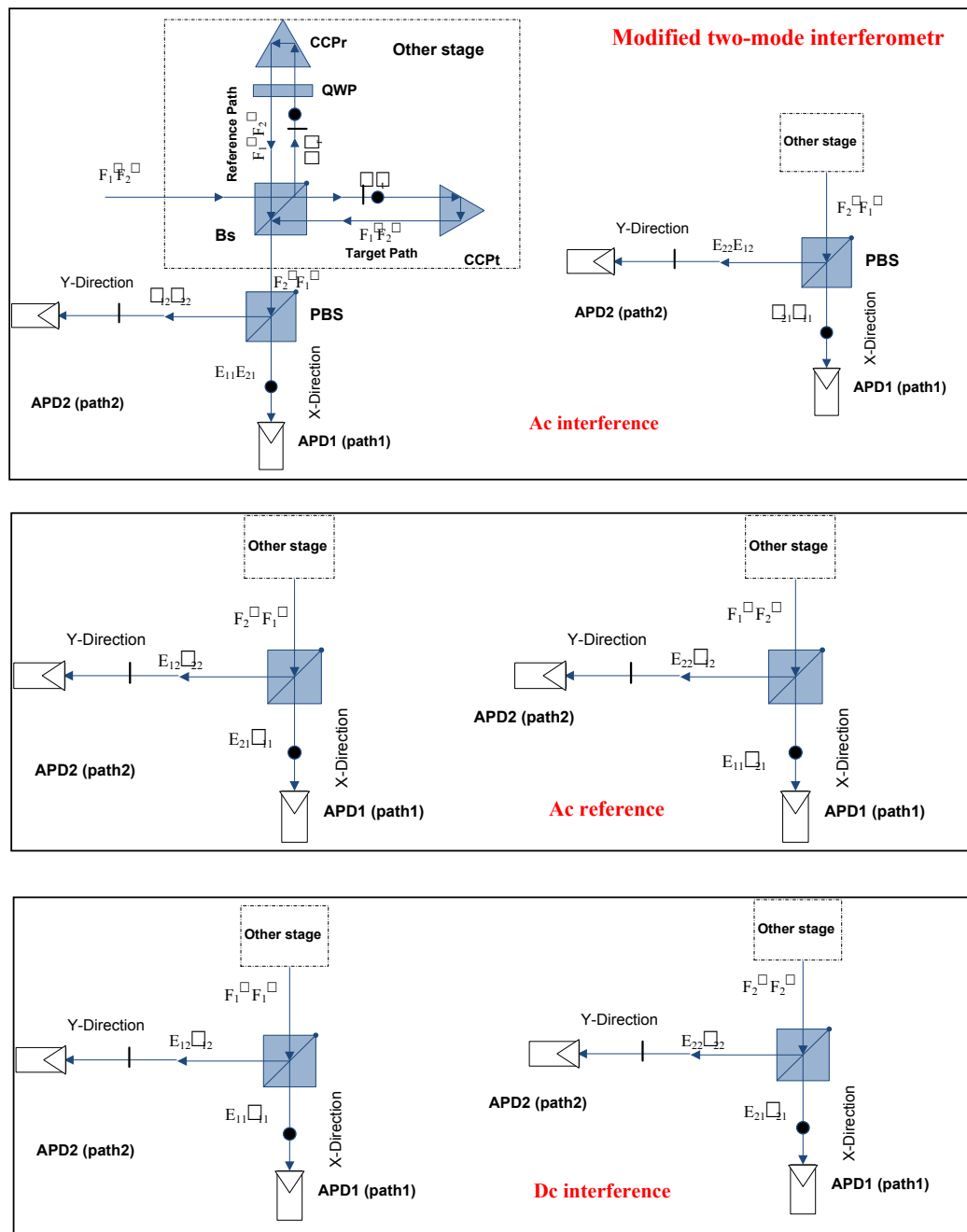


**Figure 6:** The schematic of interference terms for modified two-mode interferometer.

path are as follows:

$$E_{11} \cos(\omega_1 t + \varphi_r) \text{ and } E_{21} \cos(\omega_2 t + \varphi_r) \quad (2)$$

Where  $E_{11}$  and  $E_{21}$  are the field amplitudes out coming from  $f_1$  and  $f_2$  in path 1, respectively, and  $\varphi_r$  is the phase shift in the reference path. Accordingly, the domain subscripts show frequency ( $f_1$  or  $f_2$ ) and

path (path 1) respectively from left to right. In the same way, we have in target path (path 2):

$$E_{12} \cos(\omega_1 t + \varphi_t) \text{ and } E_{22} \cos(\omega_2 t + \varphi_t) \quad (3)$$

Where  $E_{12}$  and  $E_{22}$  show field domains of  $f_1$  and  $f_2$  from the path 2, respectively. Furthermore,  $\varphi_t$  is the phase shift in the target path. The photocurrent is

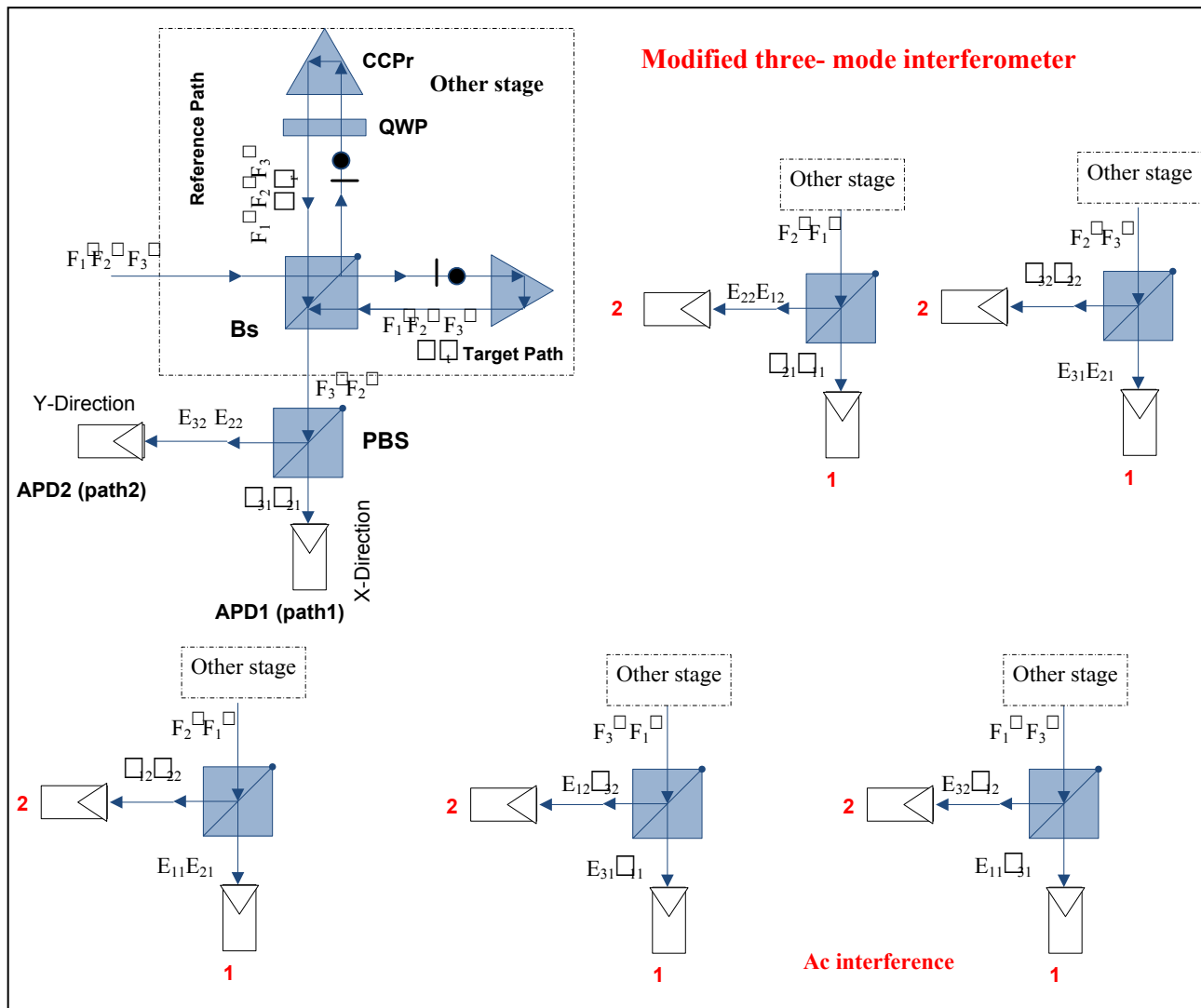


**Figure 7:** The schematic of interference terms for modified three-mode interferometer (part 1)

obtained by squaring the sum of the four F-P elements of the electric fields in which with simplifying and cancelling high frequencies off yields [34]:

$$I_m \propto (\sum E)^2 = I_D + I_A + I_R + I_\theta \quad (4)$$

Where,

$$I_D = E_1 E_2 \cos(\Delta\varphi) + E_1 E_2 \cos(\Delta\varphi) \quad (5)$$

$$I_A = E_1 E_2 \cos(\omega_b t - \Delta\varphi) + E_1 E_2 \cos(\omega_b t + \Delta\varphi) \quad (6)$$

$$I_R = E_1 E_1 \cos(\omega_b t) + E_1 E_2 \cos(\omega_b t) \quad (7)$$

$$I_\theta = \frac{E_1^2}{2} + \frac{E_2^2}{2} + \frac{E_2^2}{2} + \frac{E_r^2}{2} \quad (8)$$

Where,  $\omega_b$  is the intermode angular beat frequency and,

$$\omega_b = \omega_2 - \omega_1 \text{ and } \Delta\varphi = \varphi_r - \varphi_i \quad (9)$$

All parameters in the equations above including optical power, ac interference, dc interference, and ac reference [34] are shown in Figure 4.

### 2.2.2. F-P model of conventional three-mode interferometer

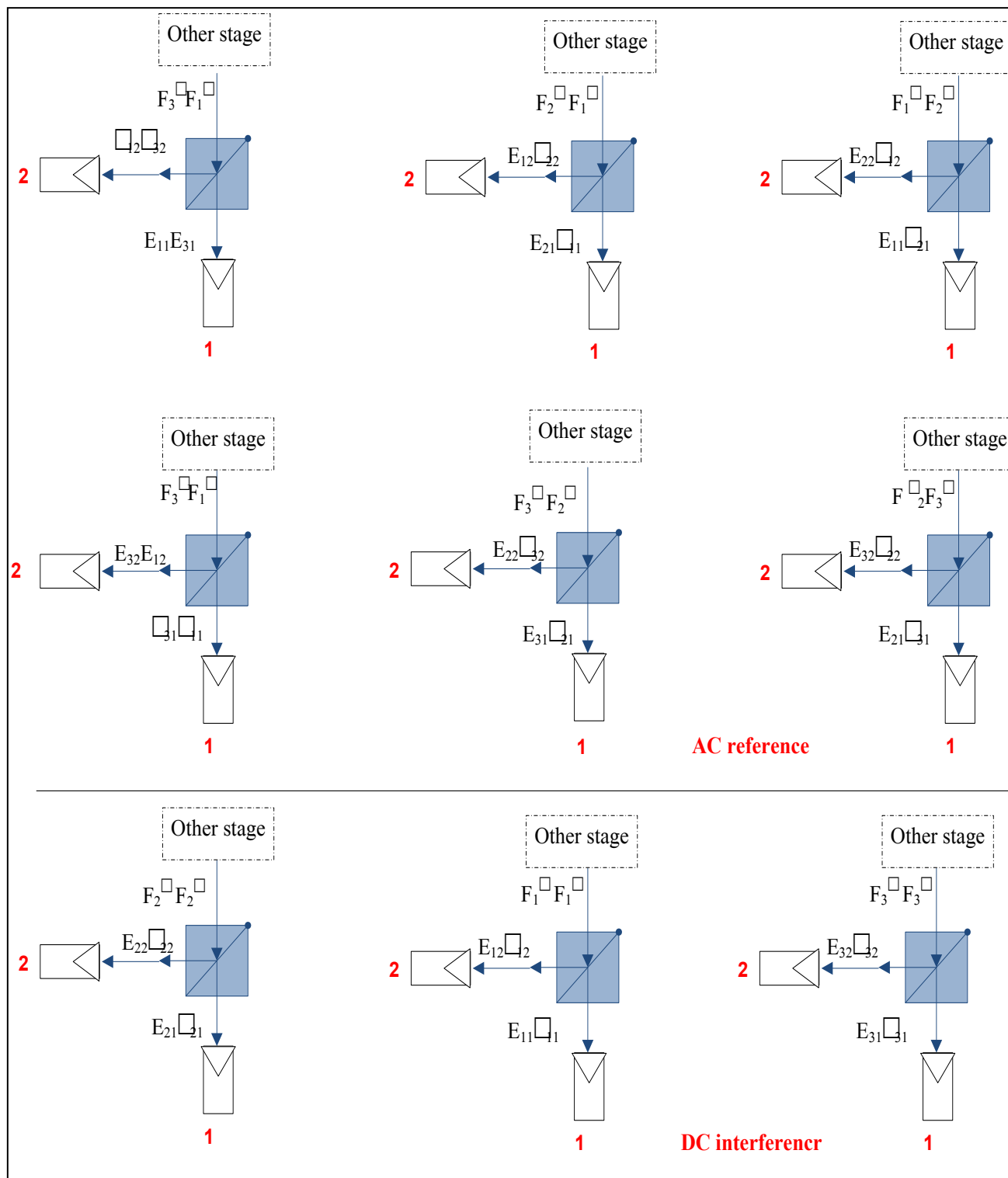
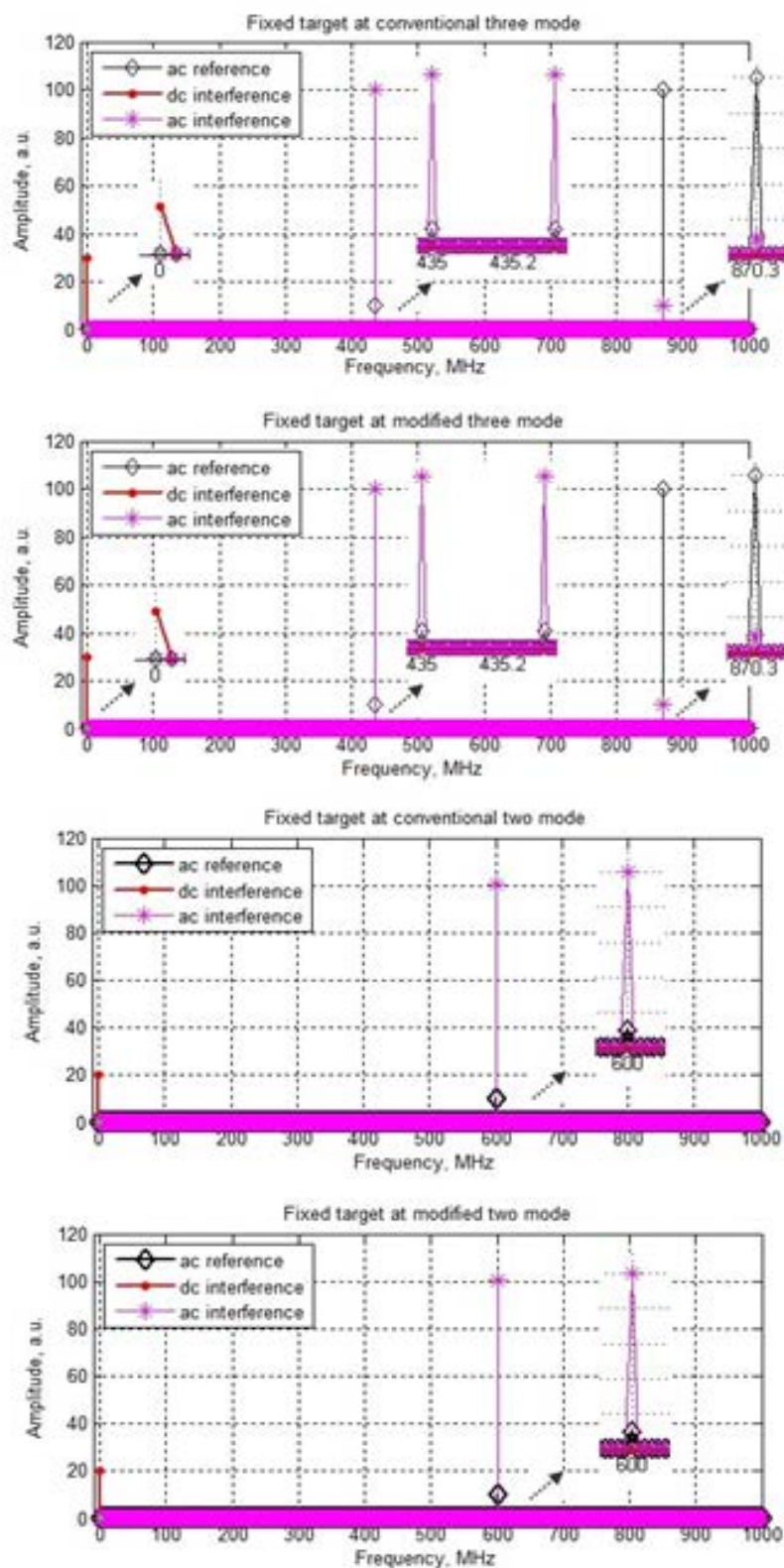
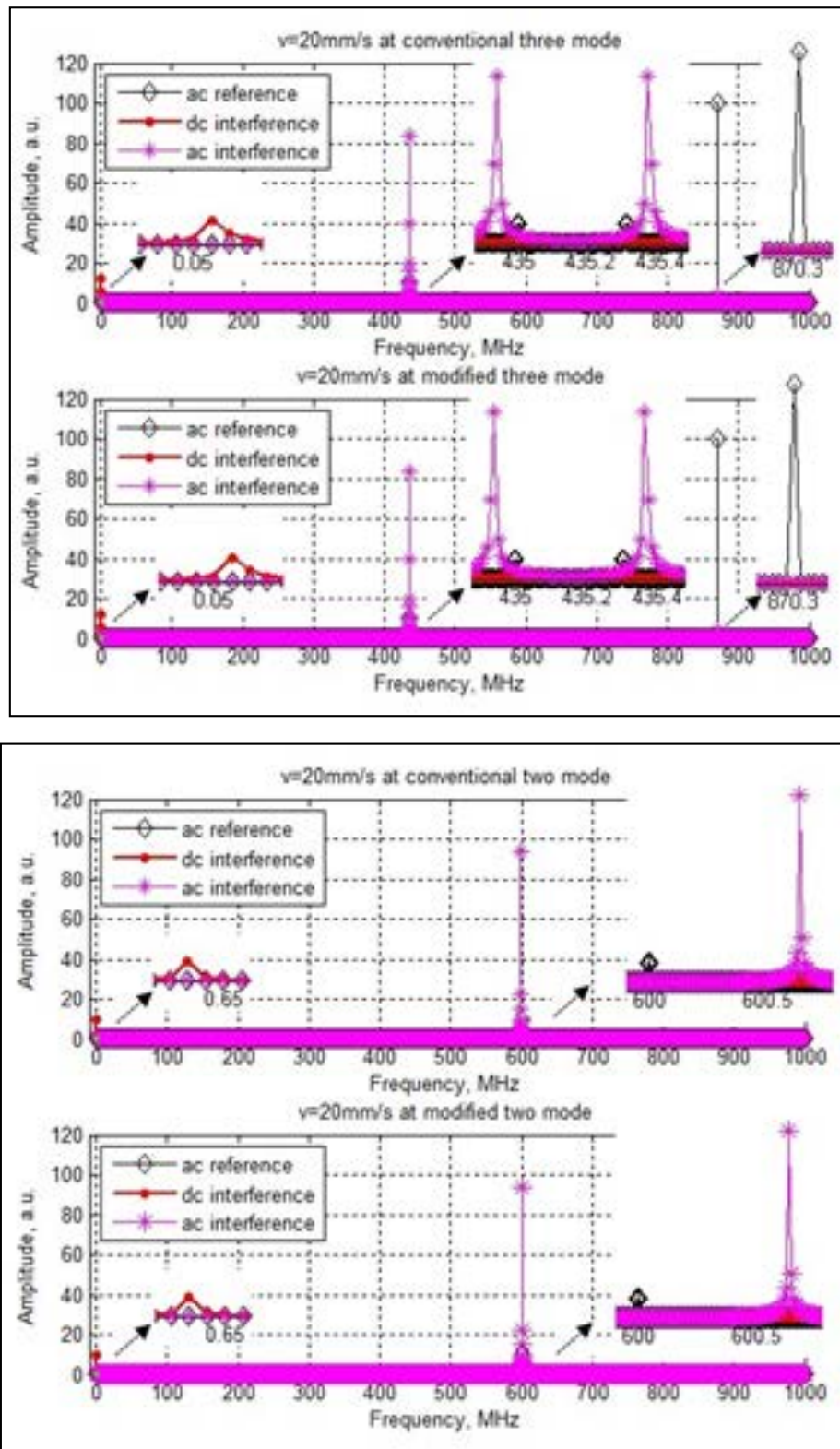


Figure 7: The schematic of interference terms for modified three-mode interferometer (part 2)



**Figure 8:** The spectrum frequency of photocurrent for zero target velocity (fixed target or static case) in four full-leakage heterodyne interferometers.



**Figure 9:** The spectrum frequency of photocurrent for low target velocity ( $v=2\text{mm/s}$ ) in four full-leakage heterodyne interferometers.

Accordingly, in the conventional three-mode superheterodyne interferometer the  $f_3$  and  $f_1$  frequencies in the reference path (path 1) are the main and  $f_2$  is the leakage frequency from the target path (path 2). The fields are as below:

$$E_{11} \cos(\omega_1 t + \varphi_r), E_{31} \cos(\omega_3 t + \varphi_r), \text{ and } E_{21} \cos(\omega_2 t + \varphi_r) \quad (10)$$

Also the frequency  $f_2$  is the main frequency in the path 2 and the other frequencies are the leakage out from path 1 into this path. Thus the resulting fields are:

$$E_{12} \cos(\omega_1 t + \varphi_r), E_{32} \cos(\omega_3 t + \varphi_r), \text{ and } E_{22} \cos(\omega_2 t + \varphi_r) \quad (11)$$

The photocurrent is obtained by squaring the sum of the six F-P elements of the electric fields explained in Eqs. (10) and (11) [36]:

$$I_m \propto (E_{11} \cos(\omega_1 t + \varphi_r) + E_{31} \cos(\omega_3 t + \varphi_r) + E_{21} \cos(\omega_2 t + \varphi_r) + E_{12} \cos(\omega_1 t + \varphi_r) + E_{32} \cos(\omega_3 t + \varphi_r) + E_{22} \cos(\omega_2 t + \varphi_r))^2 \quad (12)$$

By expanding Eq. (12), four interference terms can be given by:

$$I_{D1} = E_{11} E_{12} \cos(\Delta\varphi) + E_{21} E_{22} \cos(\Delta\varphi) + E_{31} E_{32} \cos(\Delta\varphi) \quad (13)$$

$$I_{A1} = E_{11} E_{22} \cos(\omega_L t - \Delta\varphi) + E_{11} E_{32} \cos((\omega_L + \omega_H)t - \Delta\varphi) + E_{21} E_{12} \cos(\omega_L t + \Delta\varphi) + E_{21} E_{32} \cos(\omega_H t - \Delta\varphi) \quad (14)$$

$$+ E_{31} E_{12} \cos((\omega_H + \omega_L)t + \Delta\varphi) + E_{31} E_{22} \cos(\omega_H + \Delta\varphi) \quad (15)$$

$$I_{A2} = E_{11} E_{21} \cos(\omega_L t) + E_{21} E_{31} \cos(\omega_H t) + E_{12} E_{22} \cos(\omega_L t) + E_{22} E_{32} \cos(\omega_H t) + E_{12} E_{32} \cos((\omega_L + \omega_H)t) + E_{11} E_{31} \cos((\omega_L + \omega_H)t) \quad (16)$$

$$I_{OP} = \frac{1}{2} \sum_{j=1}^2 \sum_{i=1}^3 E_{ij}^2 \quad (16)$$

Where,  $\omega_H$  and  $\omega_L$  are the high and low intermode beat frequencies, respectively:

$$\omega_H = \omega_3 - \omega_2 \text{ and } \omega_L = \omega_2 - \omega_1 \quad (17)$$

All parameters existing in the above equations are shown in Figure 5.

### 2.2.3. F-P model of modified two-mode interferometer

It is worth to note that there is no leakage in target and reference path in the modified interferometers shown in Figure 3, while, there exists leakage in the paths come after PBS (path 1 and 2). The electric fields in the path 1 are as follows:

$$E_{11} \cos(\omega_1 t + \varphi_r), E_{21} \cos(\omega_2 t + \varphi_r), \quad (18)$$

$$\tilde{E}_{21} \cos(\tilde{\omega}_2 t + \varphi_r), \text{ and } \tilde{E}_{11} \cos(\omega_1 t + \varphi_r)$$

Where  $\tilde{E}_1$  and  $\tilde{E}_2$  are the leakage fields amplitudes in path 1. The  $D_1$  photocurrent is obtained by squaring the sum of the four F-P elements of the electric fields as implied above:

$$I_1 \propto (\sum E)^2 = (E_{11} \cos(\omega_1 t + \varphi_r) + E_{21} \cos(\omega_2 t + \varphi_r) + \tilde{E}_{21} \cos(\omega_2 t + \varphi_r) + \tilde{E}_{11} \cos(\omega_1 t + \varphi_r))^2 \quad (19)$$

By omitting high frequency terms, interference equation yields:

$$I_{D1} = E_1 \tilde{E}_2 \cos(\Delta\varphi) + E_1 \tilde{E}_1 \cos(\Delta\varphi) \quad (20)$$

$$I_{A1} = E_1 E_1 \cos(\omega_b t + \Delta\varphi) + \tilde{E}_1 \tilde{E}_1 \cos(\omega_b t - \Delta\varphi) \quad (21)$$

$$I_{A2} = E_1 \tilde{E}_2 \cos(\omega_b t) + E_2 \tilde{E}_1 \cos(\omega_b t) \quad (22)$$

$$I_{OP1} = \left( \frac{E_1^2}{2} + \frac{E_2^2}{2} + \frac{\tilde{E}_1^2}{2} + \frac{\tilde{E}_2^2}{2} \right) \quad (23)$$

The electric fields in the path 2 are also described as:

$$\tilde{E}_{12} \cos(\omega_1 t + \varphi_r), \tilde{E}_{22} \cos(\omega_2 t + \varphi_r), E_{22} \cos(\omega_2 t + \varphi_r), \text{ and } E_{12} \cos(\omega_1 t + \varphi_r) \quad (24)$$

Where  $\tilde{E}_1$  and  $\tilde{E}_2$  are the leakage fields amplitudes in path 2. Also, the  $D_2$  photocurrent is calculated by squaring the sum of those four F-P element electric fields:

$$I_{D2} = E_{22} \tilde{E}_{22} \cos(\Delta\varphi) + E_{12} \tilde{E}_{12} \cos(\Delta\varphi) \quad (25)$$

$$I_{A2} = \tilde{E}_{12} \tilde{E}_{22} \cos(\omega_b t + \Delta\varphi) + E_{12} E_{22} \cos(\omega_b t - \Delta\varphi) \quad (26)$$

$$I_{A2} = \tilde{E}_{12} E_{22} \cos(\omega_b t) + \tilde{E}_{22} E_{12} \cos(\omega_b t) \quad (27)$$

$$I_{OP2} = \left( \frac{\tilde{E}_{12}^2}{2} + \frac{\tilde{E}_{22}^2}{2} + \frac{E_{12}^2}{2} + \frac{E_{22}^2}{2} \right) \quad (28)$$

The four parameters existing in these equations are shown in Figure 6.

### 2.2.4. F-P model of modified three-mode interferometer

In the modified three-mode interferometer, the interference terms in both paths 1 and 2 are computed as following. There are six fields in the modified three-mode interferometer including:

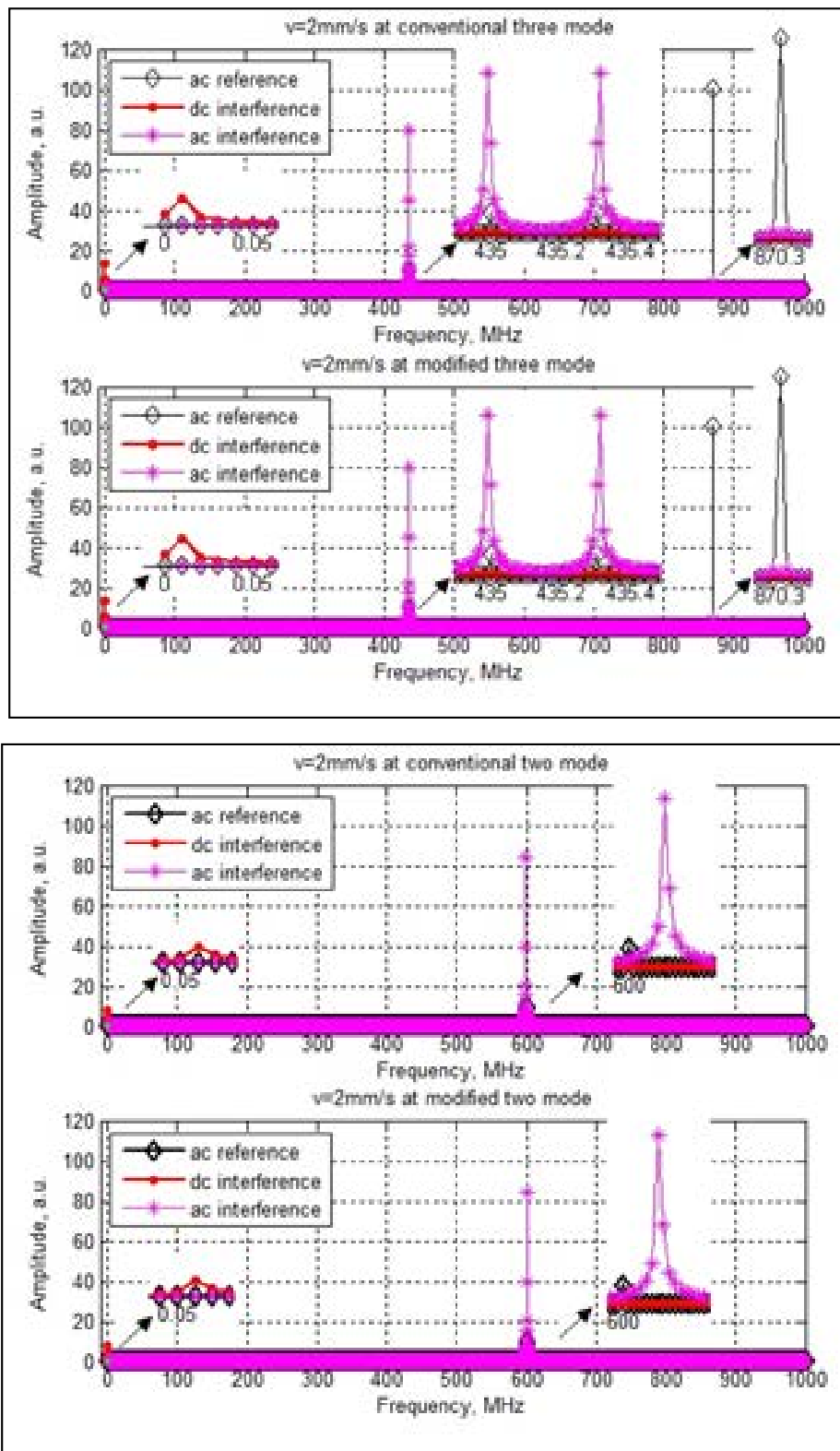


**Figure 10:** The spectrum frequency of photocurrent for high target velocity in four full-leakage heterodyne interferometers.

$$E_{11} \cos(\omega_1 t + \varphi_r), E_{31} \cos(\omega_3 t + \varphi_r), E_{21} \cos(\omega_2 t + \varphi_r), \tilde{E}_{21} \cos(\omega_2 t + \varphi_r), \quad (29)$$

$$\tilde{E}_{11} \cos(\omega_1 t + \varphi_r), \text{ and } \tilde{E}_{31} \cos(\omega_3 t + \varphi_r)$$

Where  $\tilde{E}_{31}$ ,  $\tilde{E}_{11}$ , and  $\tilde{E}_{21}$  are the leakage fields domains in path1. The  $D_1$  photocurrent is obtained by squaring the sum of the six F-P element electric fields:

$$I_{D1} = E_{21} \tilde{E}_{21} \cos(\Delta\varphi) + E_{11} \tilde{E}_{11} \cos(\Delta\varphi) + E_{31} \tilde{E}_{31} \cos(\Delta\varphi) \quad (30)$$

$$I_{A1} = E_{11} \tilde{E}_{31} \cos((\omega_H + \omega_L)t - \Delta\varphi) + E_{21} \tilde{E}_{11} \cos((\omega_H + \omega_L)t + \Delta\varphi) + E_{11} E_{21} \cos((\omega_L)t - \Delta\varphi) \quad (31)$$

$$+ E_{31} E_{21} \cos(\omega_H t + \Delta\varphi) + \tilde{E}_{31} \tilde{E}_{21} \cos(\omega_H t - \Delta\varphi) + \tilde{E}_{11} \tilde{E}_{21} \cos(\omega_L t + \Delta\varphi)$$

$$I_{AR1} = E_{11} E_{31} \cos((\omega_H + \omega_L)t) + \tilde{E}_{31} \tilde{E}_{11} \cos((\omega_H + \omega_L)t) + E_{11} \tilde{E}_{21} \cos(\omega_L t) \quad (32)$$

$$+ E_{31} \tilde{E}_{21} \cos(\omega_H t) + E_{21} \tilde{E}_{11} \cos(\omega_L t) + E_{21} \tilde{E}_{31} \cos(\omega_H t)$$

$$I_{OP1} = \left( \frac{E_{11}^2}{2} + \frac{E_{21}^2}{2} + \frac{E_{31}^2}{2} + \frac{\tilde{E}_{11}^2}{2} + \frac{\tilde{E}_{21}^2}{2} + \frac{\tilde{E}_{31}^2}{2} \right) \quad (33)$$

Also, there are the following fields in path 2:

$$\tilde{E}_{12} \cos(\omega_1 t + \varphi_r), \tilde{E}_{32} \cos(\omega_3 t + \varphi_r), \tilde{E}_{22} \cos(\omega_2 t + \varphi_r), E_{22} \cos(\omega_2 t + \varphi_r), \quad (34)$$

$$E_{12} \cos(\omega_1 t + \varphi_r), \text{ and } E_{32} \cos(\omega_3 t + \varphi_r)$$

The output current of the detector  $D_2$  becomes:

$$I_{D2} = E_{22} \tilde{E}_{22} \cos(\Delta\varphi) + E_{12} \tilde{E}_{12} \cos(\Delta\varphi) + E_{32} \tilde{E}_{32} \cos(\Delta\varphi) \quad (35)$$

$$I_{A2} = \tilde{E}_{12} E_{32} \cos(-(\omega_H + \omega_L)t + \Delta\varphi) + \tilde{E}_{22} E_{12} \cos((\omega_H + \omega_L)t + \Delta\varphi) + \tilde{E}_{12} \tilde{E}_{22} \cos(-(\omega_L)t + \Delta\varphi) \quad (36)$$

$$+ \tilde{E}_{32} \tilde{E}_{22} \cos(\omega_H t + \Delta\varphi) + E_{32} E_{22} \cos(-\omega_H t + \Delta\varphi) + E_{12} E_{22} \cos(\omega_L t + \Delta\varphi)$$

$$I_{AR2} = \tilde{E}_{12} E_{32} \cos((\omega_H + \omega_L)t) + E_{32} E_{12} \cos((\omega_H + \omega_L)t) + \tilde{E}_{12} E_{22} \cos(\omega_L t) \quad (37)$$

$$+ E_{12} E_{22} \cos(\omega_H t) + \tilde{E}_{22} E_{12} \cos(\omega_L t) + \tilde{E}_{22} E_{32} \cos(\omega_H t)$$

$$I_{OP2} = \left( \frac{\tilde{E}_{12}^2}{2} + \frac{\tilde{E}_{22}^2}{2} + \frac{\tilde{E}_{32}^2}{2} + \frac{E_{12}^2}{2} + \frac{E_{22}^2}{2} + \frac{E_{32}^2}{2} \right) \quad (38)$$

The four parameters existing in these equations are shown in Figure 7. A brief comparison between frequency-path models of implied four systems is listed in Table 1.

### 3. SIMULATION RESULTS

By drawing the frequency spectrum of photocurrents, each of interference terms stated in the previous equations will be revealed. The frequency spectrum of photocurrents of the implied four heterodyne interferometers while target is at static case is shown in Figure 8. As shown in this figure, ac interference and ac reference components are exposed in the beat frequency in this target state, while dc interference

and optical power are exposed in zero frequency [34,36].

Figures 9 and 10 show frequency spectra of photocurrents in high (20mm/s) and low (2mm/s) target velocities, respectively. With regarding to these figures, it can be concluded that ac reference stays unchanged against of the target velocity. Furthermore, conventional interferometers and its corresponding modified interferometers have the same frequency spectrum of photocurrent. The only difference between these two interferometers is the leakage components in the modified interferometers that show itself in the output of photodetectors, while in the conventional ones it reveals in the output of only one of the photodetectors.

## 4. CONCLUSION

The frequency-path models have been designed and analyzed for four nano-metrology systems based on conventional and modified laser interferometers. We showed that these models were used for representing of frequency leakage in different optical paths. Besides, the F-P model was used for nonlinearity error analysis caused by polarizing beam splitter. Comparing the modified and the conventional interferometers revealed that the number of active F-P elements and output interference terms for conventional and modified two-mode interferometer was respectively 4 and 10, but in conventional and modified three-mode ones was 6 and 21, respectively. These terms included optical power, ac interference, dc interference, and ac reference. Each of these terms has been shown in frequency spectrum of photocurrent in four heterodyne interferometers.

## REFERENCES

1. Lee, S. C., Heo, G. H. and You, K. H., "Adaptive TLS for nonlinearity compensation in laser interferometer", *International Journal of Control and Automation*, Vol. 2, (2009), pp. 31-40.
2. Schattenburg, M. L. and Smith, H. I., "The critical role of metrology in nanotechnology", *SPIE Proceedings*, Vol. 4608, (2001), pp. 116-124.
3. Sutton, C. M., "Non-linearity in length measurement using heterodyne laser Michelson interferometry", *Journal of Physics E: Sci. Instrum.*, Vol. 20, (1987), pp. 1290-1292.
4. Bitou, Y., "Polarization mixing error reduction in a two-beam interferometer", *Optical Review*, Vol. 9, (2002), pp. 227-229.
5. Dahlquist, J. A., Peterson, D. G. and Culshaw, W., "Zeeman laser interferometer", *Applied Physics Letter*, Vol. 9, (1966), pp. 181-183.
6. Dukes, J. N. and Gordon, G. B., "A two-hundred-foot yardstick with graduations every micro inch", *Hewlett Packard Journal*, Vol. 21, (1970), pp. 2-7.
7. Eberhardt, F. J. and Andrews, F. A., "Laser heterodyne system for measurement and analysis of vibration", *J. Acoust. Soc. Am.*, Vol. 48, (1970), pp. 603-609.
8. Fathi, M. T. and Donati, S., "Simultaneous measurement of thickness and refractive index by a single-channel self-mixing interferometer", *IET Optoelectronics*, Vol. 6, (2011), pp. 7-12.
9. Yazdani-rad, R., Rahaei, M. B., Kazemzadeh, A. and Hasanzadeh, M. R., "Synthesis and characterization of nanocrystalline  $Ni_3Al$  intermetallic during mechanical alloying process", *International Journal of Engineering*, Vol. 25, (2012), pp. 89-97.
10. Vaezi, M. R., Nikzad, L. and Yazdani, B., "Synthesise of  $CoFe_2O_4$ -polyaniline nanocomposite and evaluation of its magnetic properties", *International Journal of Engineering*, Vol. 22, (2009), pp. 381-386.
11. Olyae, S., Abadi, M. S. E., Hamedi, S. and Finizadeh, F., "Refractive index determination and nonlinearity modeling in fuel cells using laser heterodyne interferometer", *International Journal of Hydrogen Energy*, Vol. 36, (2011), pp. 13255-13265.
12. Milesi, I., Norgia, M., Pompilio, P. P., Svelto, C. and Dellaca, R. L., "Measurement of local chest wall displacement by a custom self-mixing laser interferometer", *IEEE Transactions on Instrumentation and Measurement*, Vol. 60, (2011), pp. 2894-2901.
13. Ghalamestani, S. G., Hilgert, T., Vandeveld, L., Dirckx, J. and Melkebeek, J., "Magnetostriction measurement by using dual heterodyne laser interferometers", *IEEE Transactions on Magnetics*, Vol. 46, (2010), pp. 505-508.
14. Zagar, B. G., "A laser-interferometer measuring displacement with nanometer resolution", *IEEE Transactions on Instrumentation and Measurement*, Vol. 43, (1994), pp. 332-336.
15. Eom, T. B., Kim, J. A., Kang, C., Park, B. C. and Kim, J. W., "A simple phase-encoding electronics for reducing the nonlinearity error of a heterodyne interferometer", *Measurement Science and Technology*, Vol. 19, (2008), pp. 1-6.
16. Noboru, N., "Heterodyne interferometers using orthogonally polarized and two-frequency shifted light sources with super-high extinction ratio", *Optical Review*, Vol. 6, (1999), pp. 443-448.
17. Hou, W., "Optical parts and the nonlinearity in heterodyne interferometers", *Precision Engineering*, Vol. 30, (2006), pp. 337-346.
18. Eom, T. B., Choi, T. Y., Lee, K. H., Choi, H. S., Lee, S., "A simple method for the compensation of

- the nonlinearity in the heterodyne interferometer”, *Measurement Science and Technology*, Vol. 13, (2002), pp. 222–225.
19. Hou, W., Zhang, Y. and Hu, H., “A simple technique for eliminating the nonlinearity of a heterodyne interferometer”, *Measurement Science and Technology*, Vol. 20, (2009), pp. 1-6.
  20. Olyaei, S., Ebrahimpour, R. and Hamedi, S., “Modeling and compensation of the periodic nonlinearity in two-mode laser heterodyne interferometer by using stacked generalization method”, *IETE Journal of Research*, Vol. 56, (2010), pp. 102-110.
  21. Cosijns, S. J. A. G., Haitjema, H. and Schellekens, P. H. J., “Modeling and verifying non-linearities in heterodyne displacement interferometry”, *Precision Engineering*, Vol. 26, (2002), pp. 448-455.
  22. Kim, H. S. and Schmitz, T. L., “Periodic error calculation from spectrum analyzer data”, *Precision Engineering*, Vol. 34, (2010), pp. 218-230.
  23. Hu, J., Hu, H. and Ji, Y., “Detection method of nonlinearity errors by statistical signal analysis in heterodyne Michelson interferometer”, *Optics Express*, Vol. 18, (2010), pp. 5831-5839.
  24. Joo, K., Ellis, J. D., Buice, E. S., Spronck, J. W. and Schmidt, R. H. M., “High resolution heterodyne interferometer without detectable periodic nonlinearity”, *Optics Express*, Vol. 18, (2010), pp. 1159-1165.
  25. Quenelle, R. C., “Nonlinearity in interferometer measurements”, *Hewlett-Packard Journal*, Vol. 34, (1983), p. 10.
  26. Wu, C. M. and Deslattes, R. D., “Analytical modeling of the periodic nonlinearity in heterodyne interferometry”, *Applied Optics*, Vol. 37, (1998), pp. 6696–700.
  27. Olyaei, S., Hamedi, S. and Dashtban, Z., “Efficient performance of neural networks for nonlinearity error modeling of three-longitudinal-mode interferometer in nano-metrology system”, *Precision Engineering*, Vol. 36, (2012), pp. 379-387.
  28. Guo, J., Zhang, Y. and Shen, S., “Compensation of nonlinearity in a new optical heterodyne interferometer with doubled measurement resolution”, *Optics Communications*, Vol. 184, (2000), pp. 49-55.
  29. Yokoyama, T., Yokoyama, T., Yokoyama, S. and Suzuki, N., “A subnanometric heterodyne interferometric system with improved phase sensitivity using a three-longitudinal-mode He–Ne laser”, *Measurement Science and Technology*, Vol. 12, (2001), pp. 157–162.
  30. Yokoyama, S., Yokoyama, T. and Araki, T., “High-speed subnanometric interferometry using an improved three-mode heterodyne interferometer”, *Measurement Science and Technology*, Vol. 16, (2005), pp. 1841–1847.
  31. Olyaei, S. and Nejad, S. M., “Characterization of elliptically polarized light and rotation angle of PBS in three-longitudinal- mode laser interferometer using the Jones matrices”, *Journal of Applied Sciences*, Vol. 7, (2007), pp. 2806–2811.
  32. Olyaei, S., Yoon, T. H. and Hamedi, S., “Jones matrix analysis of frequency mixing error in three-longitudinal-mode laser heterodyne interferometer”, *IET Optoelectronics*, Vol. 3, (2009), pp. 215–224.
  33. Olyaei, S. and Hamedi, S., “A low-nonlinearity laser heterodyne interferometer with quadrupled resolution in the displacement measurement”, *The Arabian Journal for Science and Engineering*, Vol. 36, (2011), pp. 279-286.
  34. Schmitz, T. L. and Beckwith, J. F., “An investigation of two unexplored periodic error sources in differential-path interferometry”, *Precision Engineering*, Vol. 27, (2003), pp. 311–322.
  35. Badami, V. and Patterson, S., “A frequency domain method for the measurement of nonlinearity in heterodyne interferometry”, *Precision Engineering*, Vol. 24, (2000), pp. 41-49.
  36. Olyaei, S. and Nejad, S. M., “Error analysis, design and modeling of an improved heterodyne nano-displacement interferometer”, *Iranian Journal of Electrical and Electronic Engineering*, Vol. 3, (2007), pp. 53-63.
  37. Olyaei, S. and Nejad, S. M., “Nonlinearity and frequency-path modeling of three-longitudinal-mode nanometric displacement measurement system”, *IET Optoelectronics*, Vol. 1, (2007), pp. 211-220.

